3D bio-inspired hierarchical discontinuous CFRP with enhanced ductility

F.Rizzo, F. Pinto, M. Meo

Material Research Centre, Department of Mechanical Engineering,

University of Bath, Bath, UK

Abstract

Discontinuous Carbon Fibre Reinforced Polymers (DCFRPs), due to their increased drapability, allow manufacturing of complex components that continuous CFRPs are unable to replicate. However, these materials might have reduced mechanical properties given by the loss of reinforcement continuity. This paper proposes a new bio-inspired pattern configuration of DCFRPs for the improvement of the mechanical properties (e.g. strain to failure and toughness) by exploiting failure mechanisms such as crack deflection and fibres pull-out, while preserving the high formability of DCFRPs. Resin pockets are introduced and arranged in specific three-dimensional patterns to mimic the hierarchical distribution of hard and soft phases typical of several biological systems. Finite Element models for three-point bending and Low-velocity impact tests were developed to optimise patterns and understand failure mechanisms experienced during static and dynamic tests. Experimental tests were carried out on the 3D hierarchical structures to prove its effectiveness in unidirectional and cross-ply CFRP stacking sequences. Good agreement was obtained between the numerical and experimental results especially in the prediction of the absorbed impact energy. The results demonstrated the effectiveness of the bio-inspired solution in improving the absorbed impact energy of CFRP while increasing drapability of existing prepreg materials.

Keywords: Ductility, impact; discontinuous fibre;

1 Introduction

Over the last ten years, Carbon Fibre Reinforced Polymers (CFRPs) structures have become common in a wide variety of structural applications including aerospace, automotive and railways in which materials with high strength-to-weight ratio are necessary to improve performance and to reduce energy consumption [1]. However, a key limitation of the extensive use of these materials is their limited drapability especially in reproducing complex geometries. Drapability or formability [2] is the ability of the uncured material to adapt its shape on a complex mould during its lamination procedure. This is, in fact, a critical parameter for the use of fibres in complex manufacturing procedures since, due to their high stiffness, they are difficult to deform and adapt on a surface parallel to their orientation. In order to overcome this drawback and increase the appeal from advanced industry for this material, several studies proposed the introduction of discontinuities along the fibres length in order to improve the material drapability [3-5]. Indeed, shortening the continuous long fibres , fibres have an increased

mobility in the location of the discontinuities [4, 6] that allows to the material to follow more extreme curvatures and profiles, and, thus, to be employed for a wider number of applications where high formability is required. However, discontinuous CFRP structures show lower in-plane mechanical properties in comparison with continuous one [7] due to their "softer" zones (discontinuities) and consequent stress intensification (notch sensitivity factor) in their location [8]. This behaviour, the intrinsic layered nature and the low impact resistance along the out-of-plane direction leads this material to be very sensitive against Barely Visible Impact Damage (BVID) under Low velocity Impact (LVI) conditions. Based on these considerations, the overdesign of the composite primary structure with a high safety factor [9] is then required and consequently, the benefits of using composite structures are partially lost.

A possible approach to overcome this limitation is the systematic design and optimisation of the discontinuities position in order to minimise the in-plane mechanical properties detriment of CFRP and guarantee its high formability during the manufacturing operations. Furthermore, discontinuities can be organised in patterns whose location and distribution can be studied and optimised to promote the introduction of a non-linear failure behaviour i.e. pseudo-plasticity [10] that similarly to plasticity into metals, it is able to create a plateau into the characteristic stress-strain curve of laminated material. This new mechanical feature can, not only, increase strain at failure, toughness and impact response of the material but also to provide for a visible warning of the structural damage allowing a prompt intervention before the sudden and catastrophic collapse of the structure.

The maximum expression of discontinuities pattern optimisation can be found in nature where several bio-composite materials can be identified in biological systems including bones [11], wood [12], molluscs exoskeleton including shrimps and abalone [13], and in the inner shell layer of mother–of pearl (nacre) of bivalve molluscs. The main function of the nacre and cuticle exoskeleton is the protection of the inner organs from external menaces. Nacre [14-16] consists of a brick-and-mortar composite structure with short aragonite (made of $CaCO_3$ agglomerates) tablets acting as rigid reinforcement embedded within organic viscoelastic matrix in which, the discontinuities between two adjacent rigid components are organised in a hierarchical architecture. This hierarchical organisation [17] spans multiple length scales from nanoscale to macroscale [18-20] and is the main reason for the interesting properties that characterise the excellent mechanical behaviour of the structure. Indeed, even if the main brittle components (aragonite rigid tablets), the nacre is able to reach high deformations [21] and in terms of ultimate strength intensity factor, it has be proven to be between 30 and 40 times tougher than monolithic aragonite. This improved toughness is due to several additional mechanisms including strain hardening, tablets pull-out, damage diffusion and crack deflection contribute to improve the toughness of the material, dissipating a higher amount of energy during the failure of the hierarchical structure. Strain hardening [22, 23] is due to the sliding of the different aragonite tablets ahead and around the open crack where both interlock and matrix friction provide a further friction factor which

increases the energy dissipation. Tablets pull-out [24] is the consequence of tablets sliding that results in the bridging of crack surfaces with a limited effect on energy dissipation via friction. The most effective mechanism of energy dissipation is the crack deflection [25, 26] due to the hierarchical arrangement of the bio-composite structure . This structure provides an efficient load transfer between the different aragonite tablets and throughout the pattern of discontinuities located between two adjacent tiles and along the thickness direction. This leads to matrix shear failure with crack surfaces that propagate around the reinforcement showing no failure during this process. Consequently, a longer crack path is generated within the structure with relative creation of a higher number of new surfaces dissipating a larger amount of energy [8] via plasticity (non-linear mechanics). Following this concept, several works have been focused on the adaptation of nacre microstructure with the development of bio-inspired hybrid composite materials using traditional ones such as CFRP [27] and GFRP [28]. Using nacre structure as inspiration and considering that the main source of its unique failure behaviour is the well-designed hierarchical structure, an adaptation process is performed by mimicking the organisation of its short reinforcement into the laminated composite. Indeed, by organising the fibrous reinforcement as the rigid component of nacre and considering the polymeric matrix as soft components, it is possible to create a discontinuities pattern inside the laminate structure. This leads to the activation of several pseudo-plastic mechanisms, typical of nacre mechanical behaviour that can increase the toughness and strain at failure of the brittle composite structure improving the impact response of the material. Attempts [27, 29] in creating an hierarchical discontinuous structure within a unidirectional CFRP laminate consists in inserting of several discontinuities as resin pattern into the CFRP structure by cutting every single ply along its width and aligning the two ends at a certain variable distance. The procedure was periodically repeated with an offset along the samples thickness by overlapping the different discontinuous layers to create a zig-zag pattern. In-plane and flexural mechanical properties of this structure were tested using uniaxial tensile and a three-points bending tests. From these, it was clear that the crack could propagate with no damage on reinforcement fibres leading to an increase of the global toughness of the material. Different configurations were tested in function of the offset distance and gap length, and good results were obtained analysing the strain at failure after tensile tests. Even though, a reduction of maximum strength was observed due to the notch sensitivity generated by the discontinuities presence.

Even though the observed results are remarkable, several manufacturing issue were evaluated during production procedure including accurate locating of discontinuities and optimal distribution of their pattern that represent a limit of the industrial application. The development of novel manufacturing procedures, including high precision laser-cut and 3D printing, in fact, can offer a solution to this production issue since they allow controlling position and finishing of resin patterns with a higher accuracy and higher freedom in the geometrical shapes than traditional manufacturing. In particular, 3D printing technologies allows the grown control of the structure during the manufacturing process adapting its architecture alongside the material fabrication.

X.Gu *et al.* [30] studied an emerging manufacturing process based on the use of 3D printing technologies to obtain a hierarchical microstructure of nacre within a laminated material. During the manufacturing procedure, two different typologies of thermoplastic resins at high and low moduli were used to simulate the reinforcement and the matrix component respectively. Each ply was then manufactured, stacking up the different layers using a cross-ply lamination sequence and the impact properties were evaluated using an impact rig. Comparing the results with a monolithic configuration the superior impact properties of hierarchical structure were shown and used to validate a numerical model. However, CFRP has no immediate applications in 3D printing technologies since the use of structural thermoplastic polymers is still under development.

Narducci *et al.* [31] used laser cut technology to create a complex and optimised pattern of CFRP tiles in order to maximise strain hardening and damage deflection phenomena. An hourglass tiles shape was optimised to add a friction component during failure via tiles-interlocking when sliding and pull-out mechanisms occur. Moreover, in order to include a crack deflection component, a pattern of discontinuities was introduced along the thickness direction by overlapping the tiles by half of their length. Three-point bending tests results were shown reporting an absence of brittle failure under out-of-plane loading conditions.

Based on literature and developing an innovative manufacturing procedure to introduce the resin pattern in cross-ply CFRP structures, this work is focused on the design and characterisation of a discontinuous bio-inspired laminated composite material showing improved impact response. By introducing and replicating the discontinuities pattern (resin pockets) along the in-plane and through-the-thickness directions of a unidirectional and cross-ply ($[0/90]_n$) CFRP structures, a 3-Dimensional (3D) hierarchical CFRP structure was realised. Different manufacturing solutions were proposed in order to optimise the introduction of the discontinuities pattern while the optimum elemental cell length was found out via trade-off between pseudo-plasticity and flexural strength and modulus. Their effectiveness was evaluated analytically via a modified composite micromechanics model and experimentally via three-point bending tests. Output data were used to validate the numerical model and tune its mechanical properties including flexural stiffness and flexural strength. Finally, an experimental impact campaign was carried out on the hierarchical impact samples in order to characterise the impact response of the bio-inspired CFRP structure and verify the mechanical properties variation. A numerical model was then developed and validated for theoretical support for pseudo-plastic behaviour improvement. In this work, the description of 3D hierarchical bio-inspired structure design and the manufacturing processes used to obtain hierarchical CFRP laminates are presented in Section 2 while Sections 3 illustrates experimental set-up, numerical modelling, results and discussion of three-point bending tests. Section 4 reports experimental set-up, numerical modelling, results and discussion of impact tests. Conclusions are reported in Section 5.

2 3D hierarchical bio-inspired structure

The nacre exoskeleton structure has been used as inspiration source to design a unique discontinuities pattern to increase the amount of energy absorbed by the laminate structure during quasi-static and LVI loading. In this work, pseudo-plasticity was obtained by inserting a pattern of discontinuities into the laminate body by interrupting the long fibre continuity of the uncured CFRP material along its in-plane direction.

Design parameters and the layout of the 3D hierarchical pattern for an elemental cell are reported in Figure 1a (side view) and Figure 1b (top view), where H (mm) is the length of the discontinuity, W (mm) is its width and D_X (mm) and D_Y (mm) are the width and length of the elemental cell respectively.

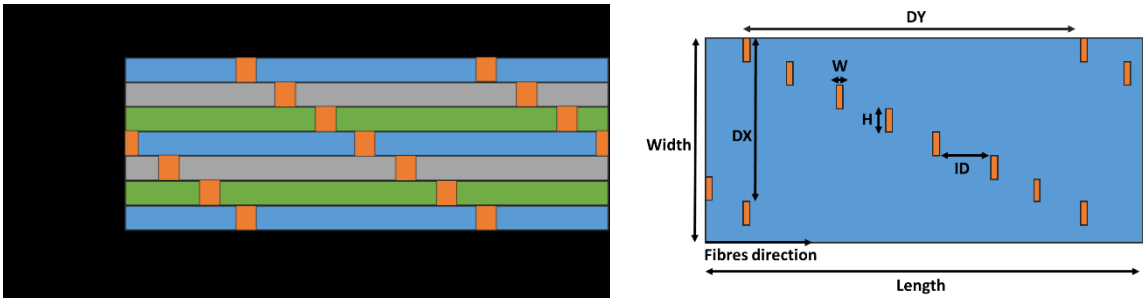

a) b)

Figure 1- Schematisation of the discontinuity pattern considered during the experimental campaign: a) side view and b) top view

Considering H and the number of plies of the structure (P_n), D_X can be defined according to Equation 1:

$$D_X = P_n H. \tag{1}$$

The length between two consecutive resin pockets is defined as Inter-discontinuity Distance ID (mm) and evaluated using the Equation 2:

$$ID = \frac{D_Y}{P_{n-1}} \tag{2}$$

Based on this in-plane pattern and imitating the out-of-plane distribution of the hierarchical bio-structure of the nacre [32], the final bio-inspired structure was created by reproducing the same distribution of resin pockets along the stacking sequence and, shifting and overlapping two consecutive layers by an offset distance ID along D_Y direction.

A representation of the patterns shifting procedure is illustrated in Figure 2 for the first three layers.

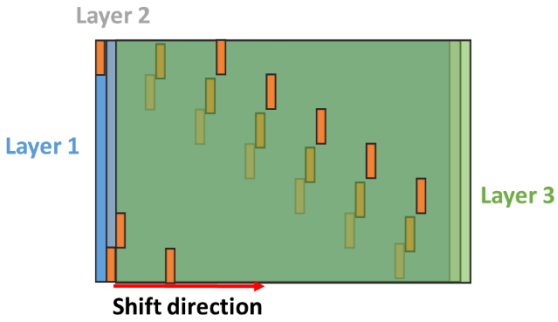

Figure 2- Layout of pattern shift along the thickness of the laminate. The pattern shift distance is ID.

Composite micro mechanic of the lamina [33] is able to predict with a certain accuracy the mechanical properties of a unidirectional laminated composite under several constitutive hypotheses including uniform average stress distribution within the fibres, roughly hexagonal fibres packing; isotropic, homogenous, void-free and linearly-elastic matrix; and homogenous, regularly-spaced, linearly-elastic fibres, following the equations below:

$$E_c = E_f V_f + E_m V_m \quad 3)$$

$$\sigma_c = \sigma_{fu} V_f + \sigma_{mu} V_m. \quad 4)$$

Where: V_f, E_f and σ_{fu} are the fibre volume fraction (0.6), the Young's modulus (~260-290 GPa) and the maximum tensile stress (~2500-2900 MPa) of the fibres, respectively; V_m, E_m and σ_{mu} are matrix volume fraction, elastic modulus (~1-5 GPa) and tensile matrix strength (~70-120MPa) respectively.
The creation of the resin pattern within the laminated structure changes the nature of the material since the continuity of the fibres is lost and a discontinuous structure is obtained leading to the loss of validity for Equation 3 and 4. Consequently, in order to predict the average mechanical properties (elastic modulus and strength) of this system, an alternative analytical model is proposed.
Using the definition of critical fibre length (l_c), it is possible to define the minimum length for fibres to transfer efficiently load and be effective in the reinforcement process [34]:

$$l_c = \sigma_{fu} d_f \backslash 2\tau_i \quad 5)$$

where τ_i is the interface shear strength (~10-40MPa) and d_f is the fibres diameter (~1-50 μm, resulting in a critical length of 1 mm. When the reinforcement fibres are continued and well-distributed along the single lamina, the fibre length (l) is $l > l_c$, and the fibres are an active component in transferring and tolerating load, while if $l < l_c$, the fibres are short and dispersed and therefore unable to transfer efficiently the load making the matrix properties dominant over the fibres ones.

Based on this premise, in order to allow the fibres to act as an effective reinforcement within the structure, all the used elemental cell lengths (8, 10, 20 and 50 mm) were set up to largely exceed this critical length. To evaluate the modulus and strength of such short fibrous reinforced system, a modified shear-lag theory for composite material [35, 36] is used taking into account the aspect ratio of the carbon fibres with the following equation:

$$E_c' = k_e E_f V_f + E_m V_m \quad (6)$$

$$\sigma_c' = k_s \sigma_{fu} V_f + \sigma_{mu} V_m \quad (7)$$

where k_e and k_s are fibre-length correction coefficients to take into account the discontinuous fibres in function of the unit cell length. The expression to define κ_e is given by Equation 8:

$$k_e = 1 - \frac{\tanh(\eta\zeta)}{\eta\zeta} \quad (8)$$

where:

$$\eta = \sqrt{\frac{E_m}{\theta(1+\nu_m)}} \quad (9)$$

$$\theta = E_f \ln(0.42\sqrt{V_f}) \quad (10)$$

$$\zeta = \frac{l}{d_f}. \quad (11)$$

Under the same hypothesis, the fracture-based correction coefficient κ_s [37] is defined as:

$$\kappa_s = 1 - \frac{\varphi}{2\zeta} - \frac{12.5}{\zeta\varphi} + \frac{5\sigma_{mu}}{\zeta\sigma_{fu}} \quad (12)$$

$$\varphi = \frac{\sigma_{fu}}{2\tau_i}. \quad (13)$$

It is important to notice that for high values of ζ (aspect ratio), both coefficients tend to 0, leading to obtain the properties of a traditional laminate material with a continuous reinforcement (no presence of resin pattern). On the contrary, for low values of ζ, k_e and κ_s tends to 1 leading to a unreinforced laminate material since fibres are too short to tolerate and transfer load. Thus, E_c and σ_c are two functions with a lower limit corresponding to $E_m V_m$ and σ_{mu}respectively, and an upper limit corresponding to the values described by Equation 3 and Equation 4 (elastic modulus and strength respectively). Analytical data are reported in Figure 3 in which an explorative analysis is reported comparing the analytical modulus and strength trends with the flexural results obtained in this work for different fibre lengths ($l=D_Y$) (see Section 3). It is important to notice that no direct correlation is possible since analytical model reports tensile properties while the experimental results are obtained

from flexural tests, but it is still possible to compare their trend since flexural properties are related to tensile ones. Indeed, under the conditions of isotropic and homogenous material, tensile and flexural properties correspond, but in this case, due to the orthotropic nature of the material and different measurement conditions, there is a difference between their values [38]. However, the mechanical properties variation due to unit cell length is independent from the material nature and their trend correlation still holds qualitatively.

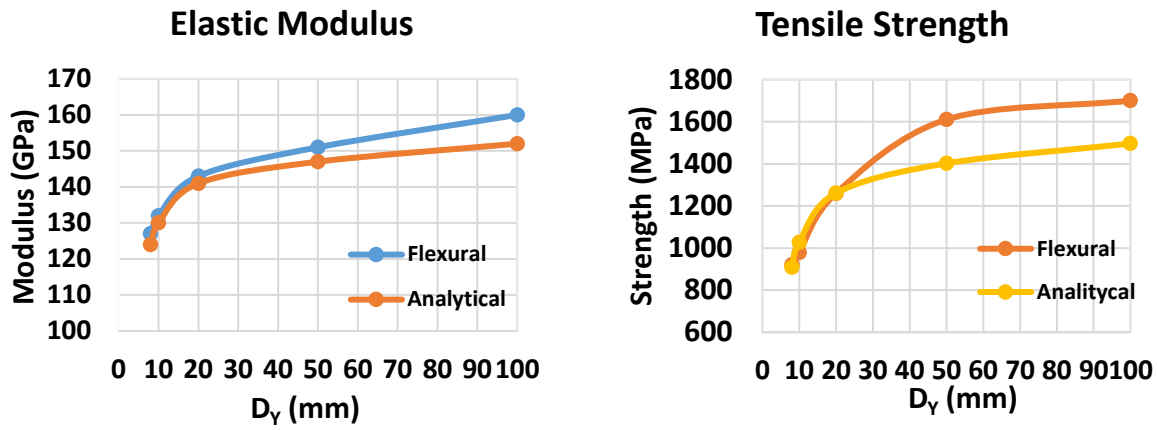

Figure 3 Variation of flexural modulus and flexural strength with D_Y alongside the analytical prediction of elastic modulus and tensile strength results

It is evident from this data that the analytical model is able to predict the trend of the mechanical properties variation (elastic modulus and strength). In particular, both these properties trends are upper asymptotic towards the reference material properties (without the presence of resin pockets pattern) for the experimental tests and E_c and σ_c (traditional composite micromechanical equations) for the analytic model. This represents an interesting data for material optimisation since the D_Y=50 mm values are close to the composite elastic modulus and strength without resin patterns (~150 GPa and 1500MPa respectively) and able to show a pseudo-plastic behaviour. However, due to the limitations of initial hypotheses, the values obtained from analytical model are overestimated but still useful to be employed as a reference for mechanical performance optimisation at different unit cell length (D_Y) and an initial condition for the validation of the numerical model developed to predict the pseudo-plastic behaviour of the hierarchical composite material. Indeed, the pseudo-plastic behaviour derived from the presence of the resin pattern introduction, is difficult to predict using an analytical model due to several complex non-linear mechanics including crack propagation, pull-out and fragmentation. However, several analytical models have been developed to predict pseudo-plastic behaviour in nacre-like structures [39, 40] but the Representative Volume Element (RVE) method for symmetrical columnar structures considered in these works is incompatible with the 3D resin pattern investigated in this work since no periodic boundary conditions can be identified for this case. Based on these considerations, in this work a numerical model was preferred to be used as reference for the design and experimental characterisation of the pseudoplastic laminates.

The introduction of the pattern of discontinuities into the laminate was carried out by following two different manufacturing procedures. In the first, named Direct Approach (DA), a specific mask was designed and manufactured with a laser cutter and used to create every single discontinuity of the in-plane pattern by cutting with a high-precision sharp blade, the CFRP fibres of the uncured material. Afterwards, during the stacking up sequence, the 3D-hierachcial design was obtained by overlapping and offsetting the in-plane structure along the out-of-plane direction. Disadvantages of DA are the formation of some defects, caused by fibre loss and non-uniform pressure during the cutting that could affect the mechanical properties. Moreover, structure configuration characterised by small D_Y values were more affected by these defects than configurations with higher D_Y values. Nevertheless, good experimental results and good correlation with numerical simulations were found for D_Y values of 50 mm that showed no influence of manufacturing defects on mechanical properties.

Following DA approach, unidirectional samples were created by cutting eight unidirectional layers 120 mm x 17.5 mm in size. Due to the geometrical parameters of the pattern, the same distribution is repeated every seven plies, therefore Ply 1 and Ply 8 are equal.

In contrast, the alternative design approach, named Indirect Approach (IA), consists in the creation of the patterns by cutting a CFRP prepreg with the length equal to the distance between two discontinuities and, afterwards, assembly of these multiple bands following a correct sequence in order to create the hierarchical structure. Following this solution, it was possible to generate the discontinuities pattern with an increased accuracy in comparison to the previous approach; however, an increase of discontinuities size was reported due to the operator limit in cutting small width for CFRP stripes. Following the IA procedure, another set of unidirectional samples were manufactured cutting 50mm x 5mm stripes of unidirectional CFRP prepreg and, organizing the single parts in function of the design parameters during the layup procedure, the same discontinuities pattern illustrated previously is obtained as a CFRP plate of 500mm x 35mm. This plate was then cut after the cure process using an abrasive blade and several samples 100mm x 17.5mm in size were obtained as reported in Figure 4.

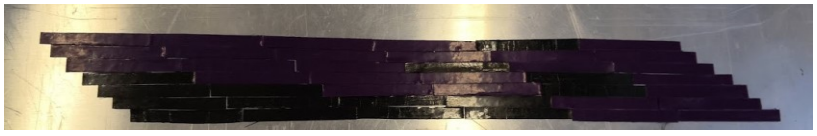

a)

Figure 4- Images of unidirectional CFRP samples using IA procedure

Based on the results obtained with unidirectional specimen, Cross-Ply (CP) CFRP samples were realised by extending the hierarchical structure concept in cross-ply CFRP laminates in order to investigate the effect of pseudo-plasticity in multidirectional composite structures. Following this premise, a cross-ply lamination sequence ($[0/90]_{nS}$) with a size of 120mm x 20mm was used to manufacture cross-ply CFRP samples. Using the DA procedure, an angular rotation of the pattern was

applied on the plies with a different fibres ordination during the discontinuities pattern creation. In particular, a rotation of 90° was applied to the pattern for 90° orientated plies to generate a consistent design of discontinues fibres inside the laminate's pattern. The rotation of the pattern had no influence on the planar shifting.

A schematisation of pattern rotation and through-the-thickness shift is illustrated in Figure 5 where the procedure is shown for the first three plies.

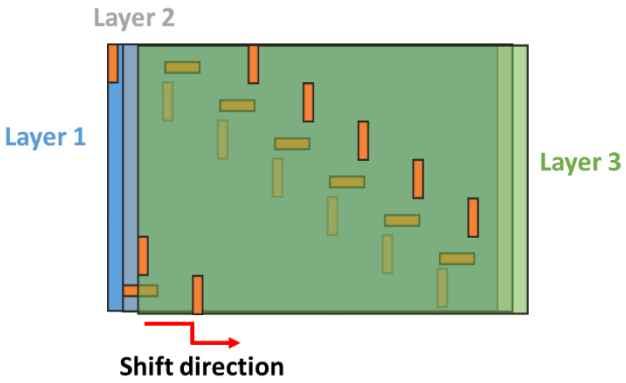

Figure 5- Layout of pattern shift along the cross-ply laminate thickness. The pattern shift distance is ID while the rotation angle is 90°.

Similarly to samples CP, impact samples were manufactured using DA manufacturing procedure with a cross-ply configuration and cut 150mm x 100mm in size as suggested by the BS EN ISO6603-1:2000 and BS EN ISO6603-2:2001 impact standards. Average thickness of the impacted samples was around 1.36 mm. Traditional CFRP laminates (with no discontinuity pattern) for each samples set were manufactured as baseline. Unidirectional CFRP prepreg (Tenax® IMS65 filament yarn with CYTEK 977-2 resin system) with a depth of 0.18 mm was used to manufacture all the samples. In order to remove air between the plies and increase the inter-ply compaction, vacuum was applied on all the uncured samples for 30 minutes and then, using an autoclave assisted curing procedure, they were processed with a pressure of 100 Psi, a temperature of 180°C with a ramp of 3 °C/min for 3 hours under vacuum. At the end of the process, an assisted cooling operation was carried out. Table 1 reports all the sample specifications involved in the experimental campaign.

Table 1-Manufactured samples specs

Sample typology	Stacking sequence	Manufacturing approach	Number of plies (L_n)	H (mm)	D_Y (mm)	D_X (mm)	Length (mm)	Width (mm)	Average thickness (mm)

Unidirectional	$[0]_8$	DA	8	2.5	8, 10, 20 ,50	17.5	120	17.5	1.23
Unidirectional	$[0]_8$	IA	8	5	50	17.5	100	17.5	1.24
Cross-ply	$[(0/90)_4/0]$	DA	9	2.5	50	20	120	20	1.38
Unidirectional reference	$[0]_8$	-	8	/	/	/	120	17.5	1.2
Cross-ply reference	$[(0/90)_4/0]$	-	9	/	/	/	120	20	1.34
Impact	$[(0/90)_4/0]$	DA	9	2.5	50	20	150	100	1.38
Impact reference	$[(0/90)_4/0]$	-	9	/	/	/	150	100	1.38

3 Three-point bending tests

Experimental set-up

In order to characterise the 3D hierarchical CFRP structure, three-points bending tests were carried out using an Instron universal tester (3369) machine and following the standard ASTM D790. A cylindrical loading nose and steel cylindrical supports with a radius of 2.5 mm were used while supports span was set at 69 mm. A cross-head speed of 6.9 mm/min was used.

Several values of D_Y were tested to identify its optimal value using a load cell of 50 kN. In Figure 6, images of experimental setup are reported.

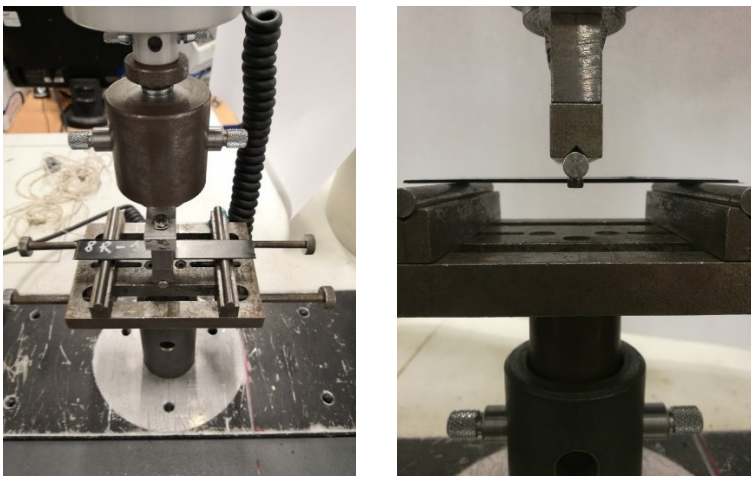

a) b)

Figure 6- Three-points bending machine set-up:a) frontal view and b) lateral view

Numerical model set-up

In order to offer a theoretical support during the manufacturing process and to allow provision of further experimental results after its validation, a Finite Element Analysis (FEA) code was developed. Using a commercial code LS-DYNA, a non-linear implicit numerical model was developed to simulate the mechanical behaviour of laminated material. Using full-integrated solid elements and orthotropic material MAT_022 (COMPOSITE_DAMAGE), 120 mm x 20 mm x 1.26 mm CFRP laminates were modelled. Similarly, resin pockets of 3D hierarchical structure were simulated using an isotropic material model MAT_024 (PIECEWISE_LINEAR_PLASTICITY) with a full-integrated solid element formulation. Erosion control was activated to remove the resin elements after failure. RIGIDWALL_CYLINDER cards were used to model the steel supports while MAT_001 (ELASTIC) with full-integrated solid element formulation was used to model the loading cylindrical nose.
Materials properties are reported in Table 2 and Table 3 where E11 and X1t are obtained via analytical model (Equation 6 and Equation 7).

Table 2- Material properties of CFRP used for FEA model. RO: density, modulus of elasticity (E11, E22, E33), poisson's ratios (PR12 ,PR31, PR32), shear modulus (G12, G23, G31), normal and transverse strength under traction and compression (X1t, X1c, X2t, X2c), shear strength (S12, S23, S31).

MATERIAL	RO (Kg/m^3)	E11 (GPa)	E22 (GPa)	E33 (GPa)	PR21	PR31	PR32	G12 (GPa)	G23 (GPa)	G31 (GPa)	X1t (MPa)	X1c (MPa)
CFRP	1560	152.6	8.9	8.9	0.0535	0.0535	0.449	4.6	3.7	3.7	1500	950

PART	X2t (MPa)	X2c (MPa)	S12 (MPa)	S23 (MPa)	S31 (MPa)
CFRP	70	250	105	89	105

Table 3- Material properties of steel and resin used for FEA model. RO: density, modulus of elasticity (E11), poisson's ratios (PR12), yeild strength (UY), tangent modulus (ETAN), effective plastic strain at failure(FAIL).

MATERIAL	RO (Kg/m^3)	E (GPa)	PR	UY (MPa)	ETAN (GPa)	FAIL
Steel	7830	210	0.3	/	/	/
Resin	1160	2	0.35	82.4	0.005	0.04

Using a penalty-based contact typology to define the interaction between the laminate and the loading nose, key parameters including friction, contact stiffness and penalty equation were defined in function of the properties of steel and CFRP and the loading nose was located in contact with the surface of the laminate. A total displacement of 13 mm was applied during the three-point bending test. Output data were collected evaluating the reaction force between CFRP surface and loading nose, and post-processed using a MATLAB code. The same numerical setup was used to develop FEA code for unidirectional samples (for DA and IA approaches). Images of the model are shown in Figure 7.

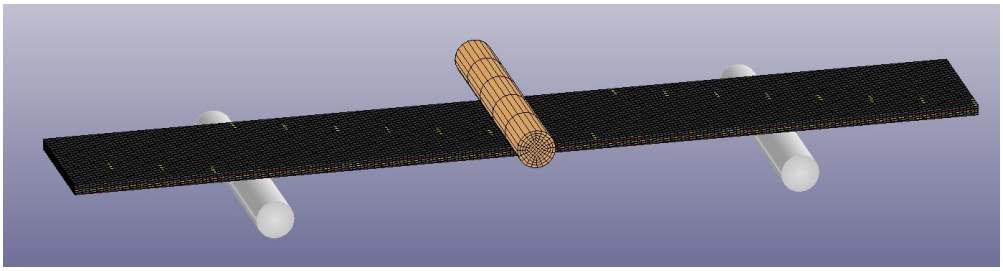

a)

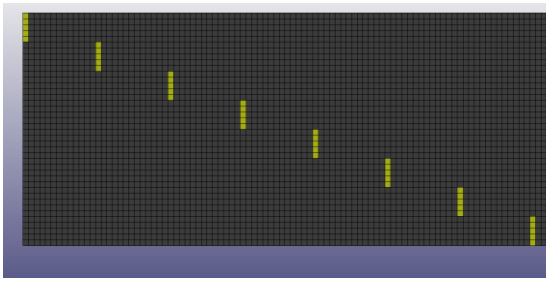

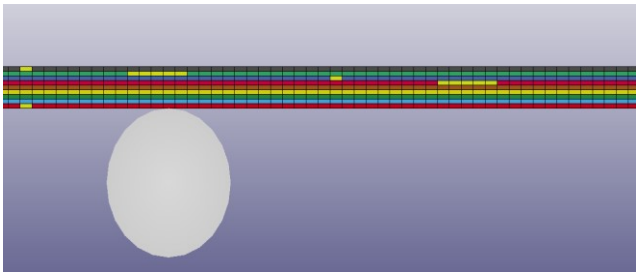

b) c)

Figure 7- FEA model layout for three-points bending: a) isometric view, b) top view and c) lateral view.

Results and discussion

The discontinuity pattern was developed to introduce a pseudo-plastic behaviour in the CFRP structure's failure mode. The causes of this behaviour are explained by the presence of stress intensification points due to the different mechanical properties between the discontinuities (resin pockets) and the surrounding areas (CFRP), and the onset of fibre pull-out and crack deflection during crack propagation. All these pseudo-plastic mechanisms are able to increase the global strain at failure and then the toughness of the structure.

Stress intensification (or notch sensitivity), as studied in fracture mechanics [41], is a mechanical phenomenon generated when a discontinuity is introduced within an uniform body. The discontinuity locally creates an area where stresses are intensified, and its effect is amplified when a regular pattern of discontinuities is introduced into the laminate [42]. When cracks are generated in correspondence with one of these discontinuities, they start to propagate through the thickness of the laminate with a convoluted path (crack deflection), following the 3D hierarchical pattern. This leads to a fragmentation of the CFRP structure and an higher amount of dissipated energy since multiple and convoluted cracks require more energy to propagate and generate new surfaces than a single crack [43]. During the CFRP fragmentation, fibre pull-out occurs due to matrix failure leading to a gradual and smooth failure behaviour that prevents a catastrophic collapse of the structure. Even though these series of mechanisms increase the toughness and strain at failure of the structure alongside reliability and safety, however, due to the presence of the discontinuities, negative effects in mechanical properties of the laminate can

be observed and, therefore, a careful design of the geometrical features of the hierarchical design is necessary.

Based on these considerations and analysing the effect of several configurations of discontinuity patterns at different D_Y values (8, 10, 20 and 50 mm), a trade-off between the flexural modulus and flexural strength, and pseudo-plasticity was carried out, supported by the analytical results of the elastic modulus and tensile strength obtained considering the modified micromechanical equations (Equation 6 and Equation 7). Indeed, analysing the curves in in Figure 9.a., the effectiveness of the introduction of the discontinuity pattern in enabling pseudo-plasticity is demonstrated by the presence of a stress plateau for all the samples configurations with no signs of brittle behaviour during failure. Increasing the size of D_Y, flexural strength and flexural modulus of the laminate increase while a decrease in extension of pseudo-plastic plateau is recorded. This is due to the dependency of these properties from the number of discontinuities introduced within the structure. Consequently, the increase of the D_Y value reduces the number of discontinuities within the structure, increasing the flexural modulus and strength of the structure. Flexural modulus and flexural strength variations with D_Y are reported in Figure 9.b. As it is possible to analyse from the curves, in fact, a value of D_Y equal to 50mm shows the highest mechanical properties and a good pseudo-plastic behaviour with a good potential for trade-off between the two variables. Flexural results of continuous CFRP sample (100 mm) are reported in Figure 9 as reference.

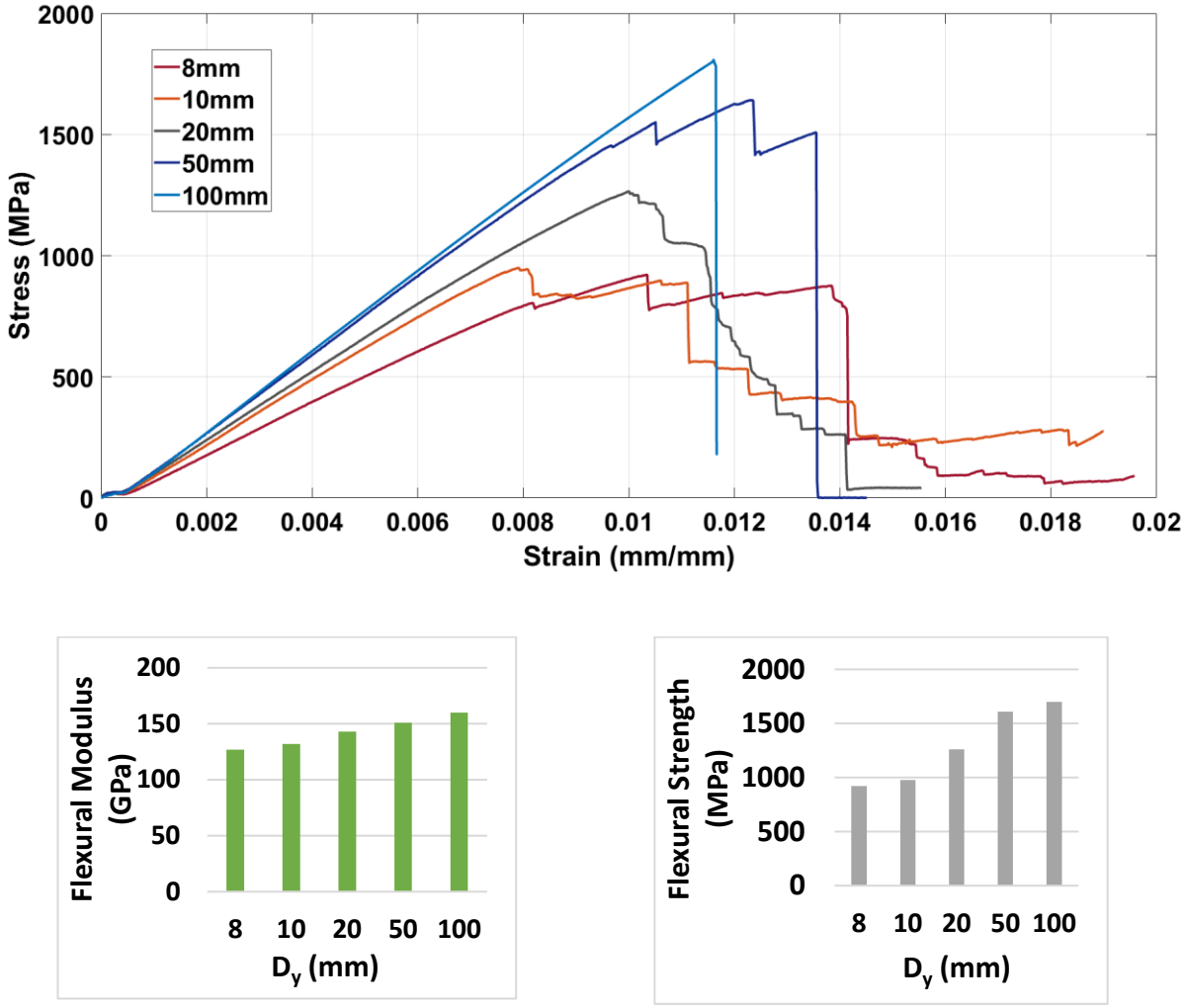

Figure 8-Experimental flexural results for unidirectional configuration (DA procedure) configuration at different D_Y values reporting flexural modulus and strength.

In order to validate the effect of the discontinuities patterns in contrast with a traditional laminate Computed Tomography (CT) scan analyses were carried out analysing the crack propagation mode in different samples. Results are shown in Figure 9.

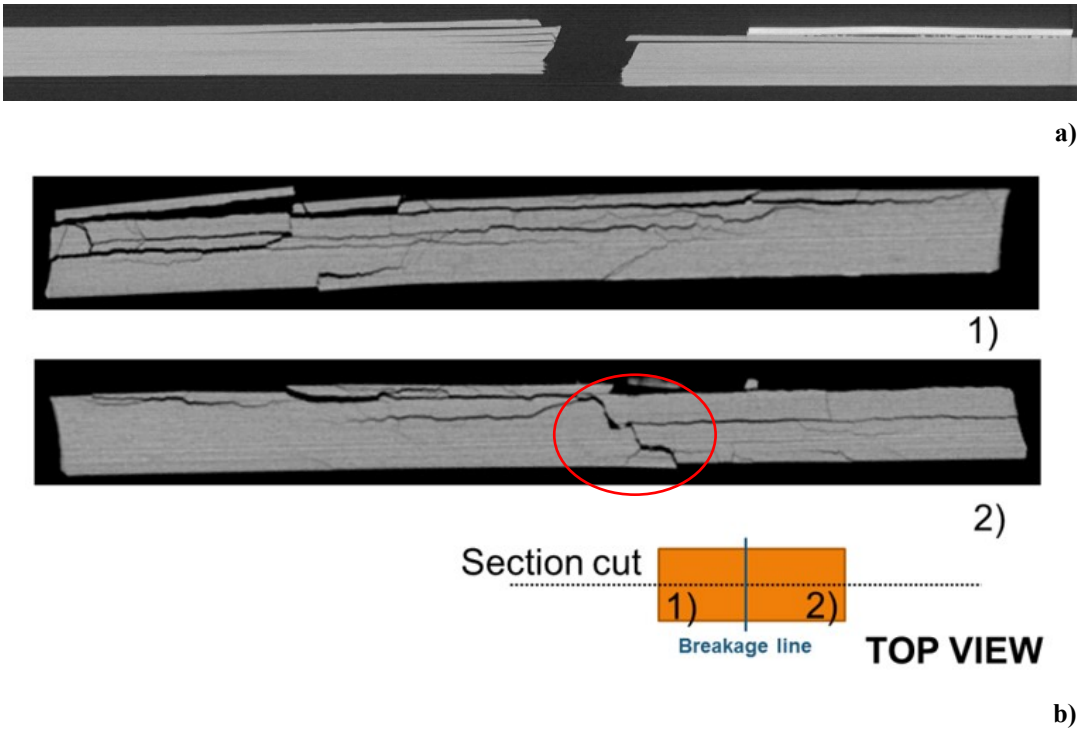

Figure 9 – CT scan images of tested samples: a) traditional CFRP reference and b) U sample where is possible to observe the crack propagation along the discontinuity pattern (red circle).

Analysing the images it is clear that they propagates through the thickness of the sample following the 3D hierarchical pattern of discontinuities (Figure 9.b). Indeed, a crack deflection mechanism with a convoluted crack path is identified since regularly spaced resin pockets allow a sort of "zig-zag" pattern, in contrast with an unprocessed material where the crack propagation is transversal to the loading section (Figure 9.a) [44]. As a consequence, a higher amount of energy is absorbed by the hierarchical CFRP since the energy required by the crack to propagate is proportional to its length [8]. Moreover, strain hardening is reported by the output data with an increase of strain at failure in comparison with a traditional CFRP structure.

Based on the experimental data, damage topology and analytical model prevision, a value of D_Y equal to 50 mm was selected for the rest of the experimental campaign as the best compromise between strength, modulus and pseudo-plasticity.

The output data of the flexural experimental campaign on 3D hierarchical structure are reported in Figure 10. FEA model is reported in the same graph.

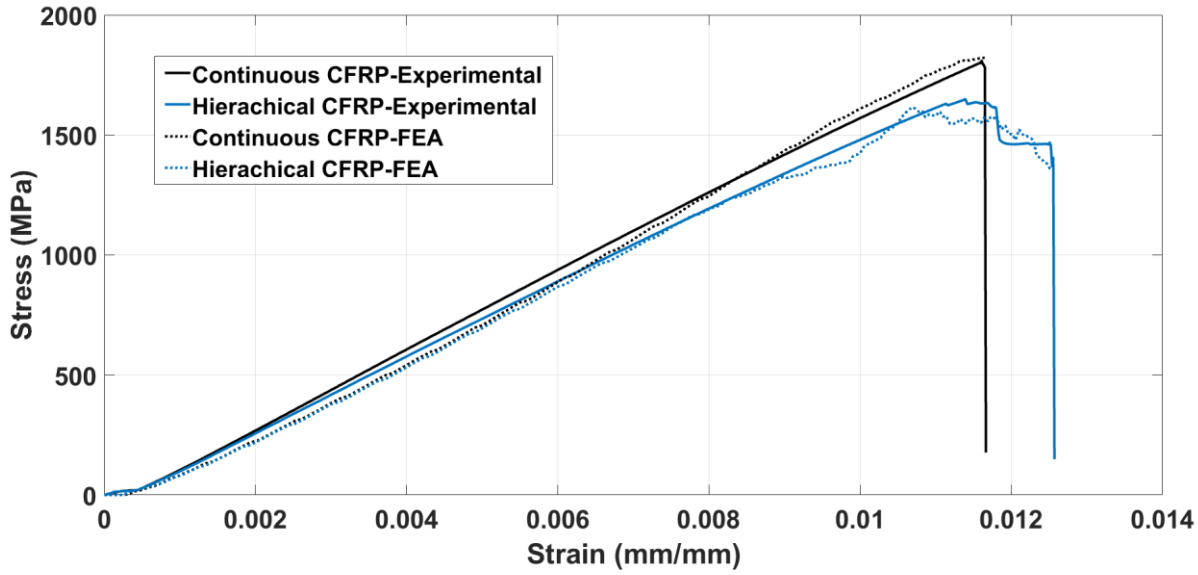

Figure 10- Experimental stress-strain curves of unidirectional configuration obtained via DA procedure. FEA stress-strain curves are reported.

Table 4 reports the statistical data from the evaluation of flexural modulus, flexural strength (first peak in the curve), flexural strain (when flexural strength is reached) and strain at failure (last peak before failure). Average and standard deviation are reported for each output parameter.

Table 4- Experimental data report for unidirectional configuration obtained via DA procedure. Mean and standard deviation for each parameter are reported.

Sample	Number of species	Energy [J]		Flexural modulus [GPa]		Flexural strength [MPa]		Flexural strain [mm/mm]		Strain at failure [mm/mm]	
		Mean	Standard dev.	Mean	Standard dev.	Mean	Standard dev.	Mean	Standard dev.	Mean	Standard dev.
Unidirectional-DA	3	10.43	0.71	157	0.0106	1640	35	0.0114	0.0002	0.0122	0.0003
U reference	3	10.31	0.3	160	0.0387	1720	67	0.0117	0.0001	/	/
Unidirectional-DA (Numerical)	/	10.40	/	155	/	1643	/	0.0114	/	0.0126	/
Unidirectional reference (Numerical)	/	10.34	/	162	/	1820	/	0.0107	/	/	/

Analysing the results, a minimal variation in comparison with traditional references of -5% for flexural strength is reported since, as illustrated previously, the presence of the discontinuity pattern compromises the structural continuity of hierarchical samples. On the contrary, a small increase of the strain at failure (+4.1%) is recorded in the comparison between 3D hierarchical structures and baselines. This is due to crack deflection and pull-out mechanism that allow the stable failure generating the stress plateau in the experimental curves. Using these experimental data, a validation of the FEA model was carried out and a good agreement between numerical and experimental results was found in mechanical response prevision.

Unidirectional samples obtained following the IA procedure are tested using the same test conditions and the output results are reported in Figure 11

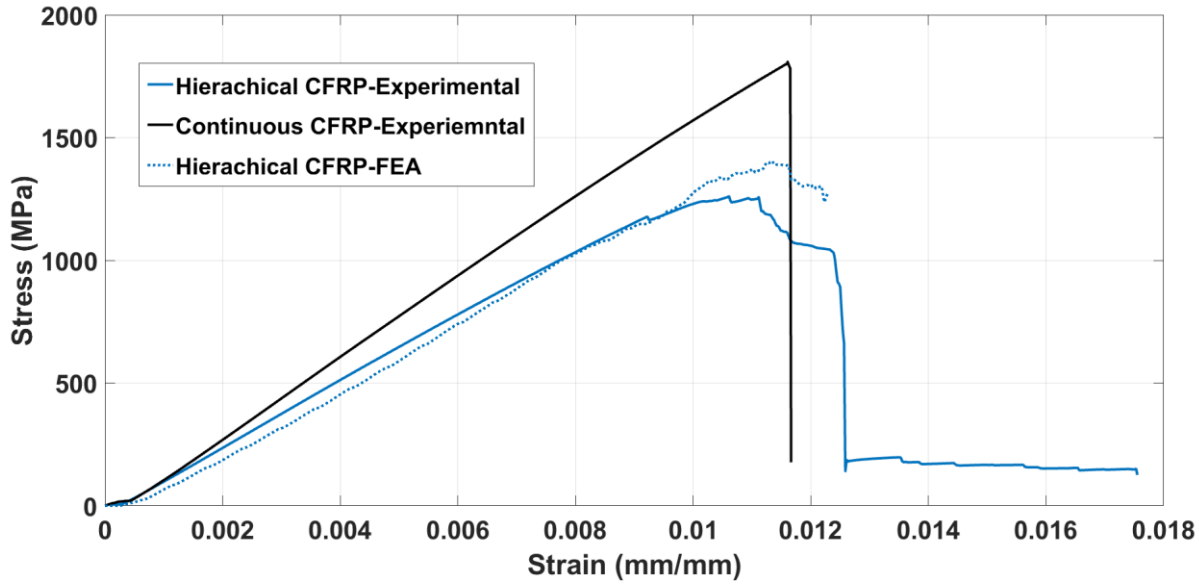

Figure 11-Experimental stress-strain curves of unidirectional configuration obtained via IA procedure. FEA stress-strain curve is reported.

The details of the output results are reported in Table 5

Table 5- Experimental data report for of unidirectional configuration obtained following IA procedure. Mean and standard deviation for each parameter are reported.

Samples	Number of species	Energy [J]		Flexural modulus [GPa]		Flexural strength [MPa]		Flexural strain [mm/mm]		Strain at failure [mm/mm]	
		Mean	Standard dev.	Mean	Standard dev.	Mean	Standard dev.	Mean	Standard dev.	Mean	Standard dev.
Unidirectional -IA	4	9.68	0.59	143	2.9	1198	77.84	0.01	0.00011	0.0127	0.00046
Unidirectional reference	3	10.31	0.3	160	3.87	1720	67	0.0117	0.0001	/	/
Unidirectional - IA (Numerical)	/	10.60	/	138	/	1234	/	0.0102	/	0.0123	/

In this case, the decrease of mechanical properties of this configuration in comparison with a traditional CFRP are more significant especially in terms of flexural modulus (-10%) and flexural strength (-30%) due to the increase of the notch sensitivity for discontinuities size (H=0.5 mm). The bigger size of the resin pockets allows having a higher strain at failure than in the hierarchical samples (+3.93%) with an increase of +7.9% on the traditional references. Hence, the pseudo-plastic behaviour is more evident for the IA unidirectional configuration.

Also, in this case, FEA model is able to predict the experimental behaviour showing a good agreement with experimental data even though an overestimation of flexural stress is reported due to numerical instabilities. Flexural modulus and strain at failure have a good correspondence with experimental data. Cross ply samples were tested using the same experimental setup. Output results are reported in Figure 12

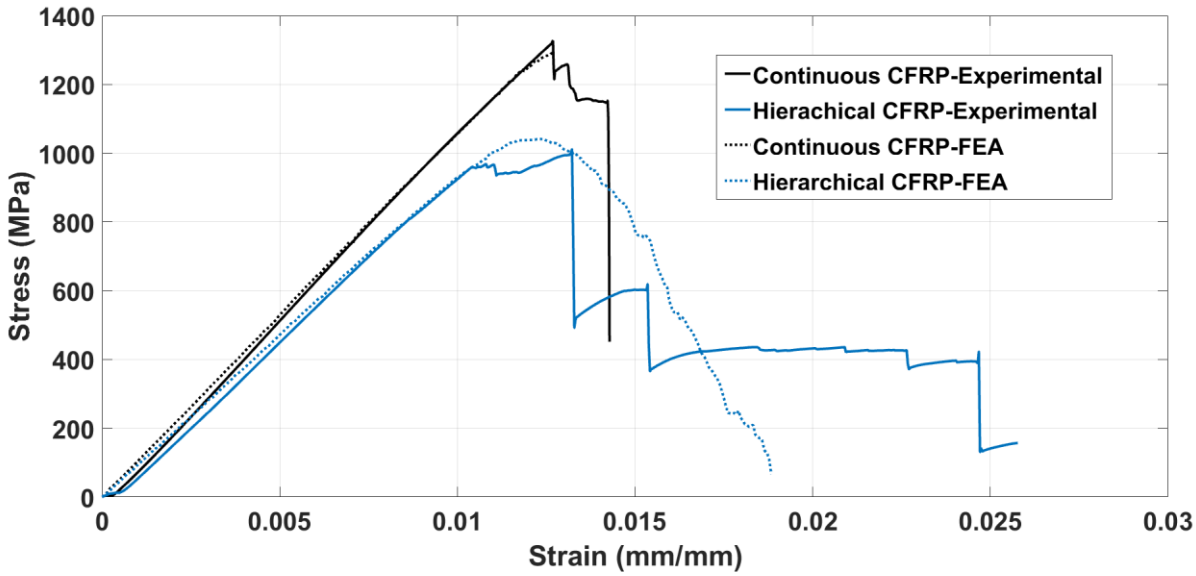

Figure 12-Experimental stress-strain curves of cross-ply configuration. FEA stress-strain curve is reported

Output details of the characteristic mechanical properties of cross-ply CFRP samples are reported in Table 6.

Table 6- Experimental data report for cross-ply configuration. Mean and standard deviation for each parameter are reported.

Sample	Number of species	Energy [J]		Flexural modulus [GPa]		Flexural strength [MPa]		Flexural strain [mm/mm]		Strain at failure [mm/mm]	
		Mean	Standard dev.	Mean	Standard dev.	Mean	Standard dev.	Mean	Standard dev.	Mean	Standard dev.
CP samples	3	12.6	2.15	98	4.8	1023	42	0.0127	9.1E-4	0.0248	0.0012
CP references	3	9.53	1.43	107	2.9	1284	179	0.0127	0.0017	0.0138	8.9E-4
CP samples (simulated)	/	11.45	/	100	/	1041	/	0.0122	/	0.0172	/
CP references (simulated)	/	8.97.	/	108	/	1291	/	0.0126	/	/	/

As shown in the data analysis, also in case of the cross-ply samples, the mechanical properties are inevitably reduced if compared with the pristine material in terms of flexural modulus and flexural strength by -8.4% and -20% respectively. However, the toughness (+24%) and the strain at failure (+44.35 %) show a remarkable increase in comparison with a cross-ply traditional CFRP. Indeed, in

this case, crack deflection mechanism is able to absorb more energy since the angle component is added to the discontinuity pattern leading to a longer and convoluted crack path. Unlike in the previous cases, the leading failure phenomenon is the delamination between plies with different orientations [45] that helps the crack propagating through the sample. In fact, due to the larger scale of the delamination phenomenon, a higher number of resin pockets are involved in the process and a higher number of cracks starts to propagate along different positions of the discontinuities pattern. In other words, delamination becomes a catalyst for crack deflection mechanism.

The trade-off between the pseudo-plastic behaviour and mechanical performance is analysed for unidirectional (DA and IA) and cross-ply configurations. The trade-off results are illustrated in Figure 13, where the effectiveness of the 3D hierarchical approach is demonstrated to have the best effects on cross-ply stacking sequence.

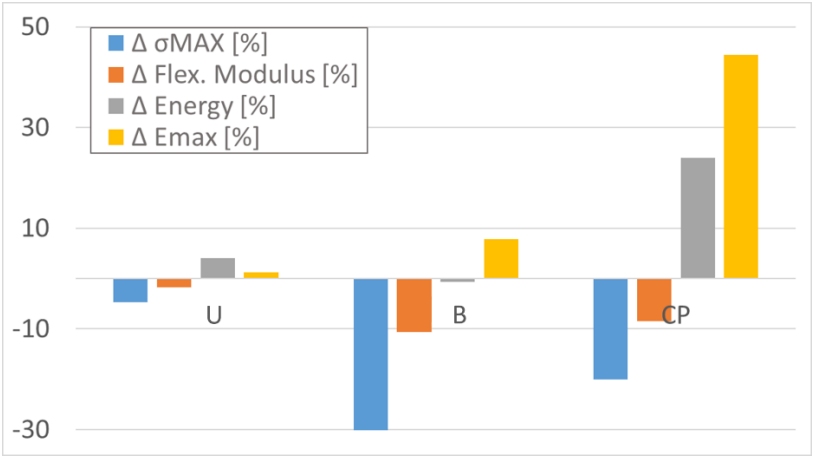

Figure 13-Trade-off between pseudo-plastic behaviour and mechanical properties of all the samples tested during the experimental campaign. The results indicate that the discontinuity pattern gives best results for complex stacking sequences rather than for unidirectional samples. U=Unidirectional with DA procedure, B=Unidirectional with IA procedure and CP=cross-ply

The FEA model is able to simulate this experimental test and have a good agreement with values of flexural modulus and maximum strength even if part of the pseudo-plastic effect is underestimated.

4 Low velocity impact tests

Experimental set-up

A drop tower machine (2.66 kg of impacting weight) was used to perform LVIs on the 3-D hierarchical samples. A hemispherical tip of 20 mm of diameter was used to apply the impact load on the samples surface using different level of: 4J, 8J and 12J with an impact velocity of 1.73 m/s, 2.45 m/s and 3.03

m/s respectively. Samples were placed into the impact machine using a clamping support in which the samples were fully constrained in order to avoid undesired vibrations.

Using a USB-PICOSCOPE Oscilloscope and a Kistler Load cell, impact data were obtained and raw load signals (Time-Volt) were collected from the oscilloscope and converted into Force-Displacement curves [46]. BS EN ISO6603-1:2000 and BS EN ISO6603-2:2001 standards were used as guidelines for impact set-up and results interpretation. Impact machine scheme and apparatus are illustrated in Figure 14.

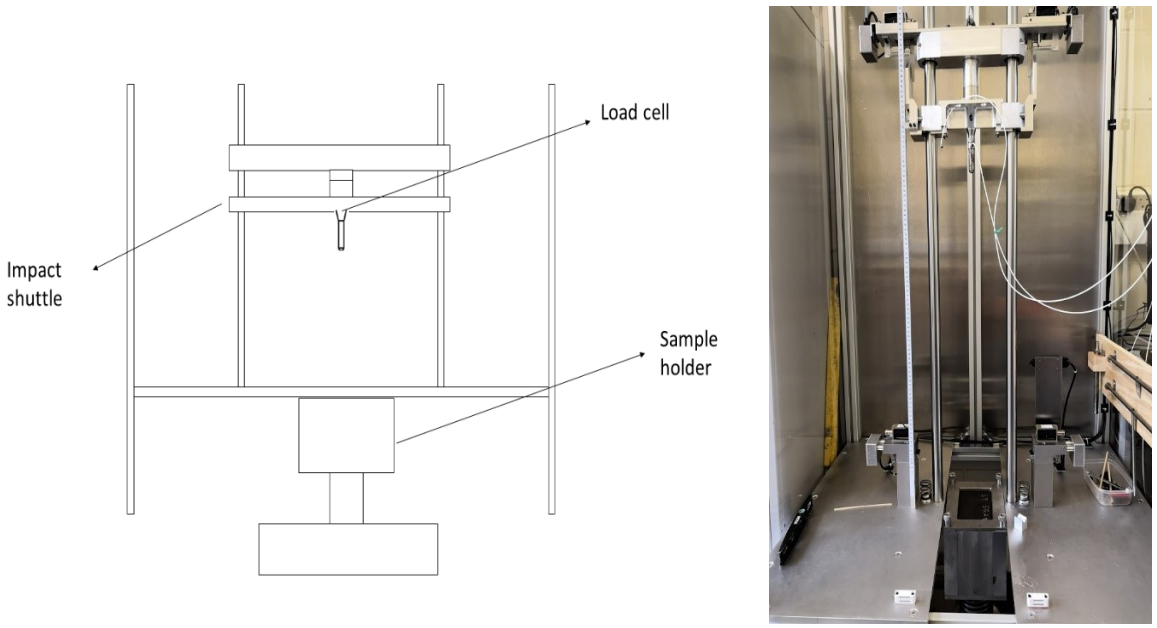

Figure 14-Impact machine used during the impact campaign: a) scheme and b) apparatus

Numerical model set-up

Once the model was validated for the three-point bending test, an explicit non-linear FEA model was developed based on a cross-ply configuration of an aeronautic laminate in order to have a prevision of the experimental data of a Low Velocity Impact (LVI) test. The size of the CFRP plate was 150 mm x 100 mm x 1.39 mm and the hemispherical impacting mass was modelled as a semi-sphere of 20 mm in diameter. A traditional CFRP plate model was developed as baseline for the impact behaviour evaluation of numerical 3D hierarchical structure. Default LS-DYNA element formulation was used for the solid elements while a Flanagan-Belytschko stiffness form formulation for hourglass control was used to control the energetic degeneration of the solid elements. LS-DYNA theory manuals [47, 48] were used for support during the model development.

Images of the model are shown in Figure 15:

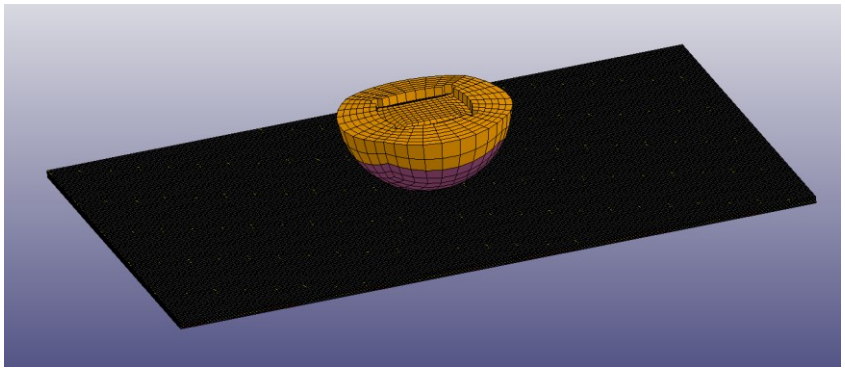

a)

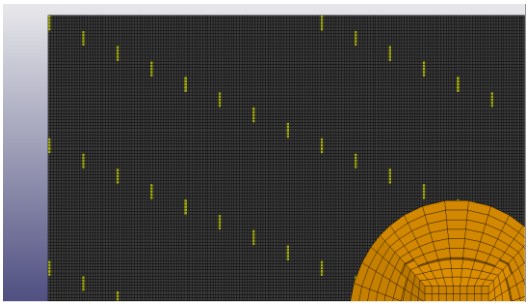

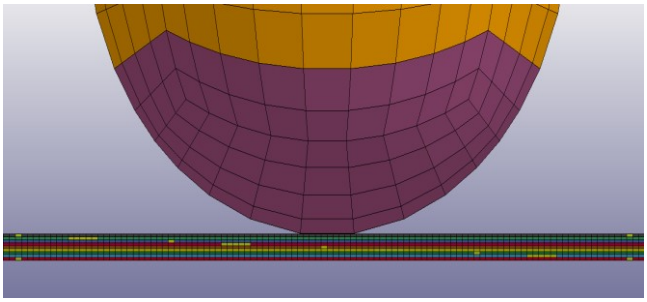

b) **c)**

Figure 15- FEA model layout for LVI test:a) isometric view, b) top view and c) lateral view.

In order to model the discontinuity pattern inside the material using MAT_024 (PIECEWISE_LINEAR_PLASTICITY) material model, mesh sizing was chosen ad-hoc to have a consistent dimension along the in-plane and out-of-plane directions with each element 0.5mm x0.5 mm x0.17 mm in size. The reason for the mesh refinements is due to the small dimensions of the discontinuities pattern (H=2.5 mm, W=0.5 mm, D_Y = 50 mm, DX=20 mm) that constrain the global mesh size of the model forcing the use of a uniform refined mesh (565100 elements in total).

It is possible to see in Figure 15.c how the discontinuities pattern changes in function of the orientation of the relative layer, as the case for the CP samples. Contact between the impacting object and CFRP plate was modelled using a PENALTY-BASED contact algorithm in which the erosion of negative volume elements was activated, while plate boundaries conditions were modelled as simple supported. To take into account the damage mode in CFRP plates, MAT_261 orthotropic material [49-51] was used to simulate the single plies of the CFRP material.

Damage prediction of fibre and matrix is defined for each element using tensile, shear and compressive strengths as activation criteria for damage initiation while, the relative toughness parameters are used as the complete failure of the single elements.

Delamination was modelled using a TIEBREAK_CONTACT model [47]. This contact is considered a tied contact before the failure criteria is satisfied. Afterwards, the contact switches its formulation into a penalty-based one. The failure criteria used in this work was a stress-based criterion with linear damage development.

MAT_261 parameters are reported in Table 7:

Table 7- MAT_261 orthotropic material card paramters:RO: density, modulus of elasticity (E11, E22, E33), poisson's ratios (PR12 ,PR31, PR32), shear modulus (G12, G23, G31), normal and transverse strength under traction and compression (X1t, X1c, X2t, X2c), shear strength (S12, S23, S31), compresisve fibre failure energy (ENKINK), tensile fibre failure energy (ENA), Intralaminar matrix tensile energy failure (ENB), Intralaminar matrix trasnverse shear energy failure (ENT) and Intralaminar matrix longitudinal shear energy failure (ENL).

PART	RO (Kg/m^3)	E11 (GPa)	E22 (GPa)	E33 (GPa)	PR21	PR31	PR32	G12 (GPa)	G23 (GPa)	G31 (GPa)	X1t (MPa)	X1c (MPa)
CFRP	1530	152	8.9	8.9	0.0535	0.0535	0.449	4.6	3.7	3.7	1500	950
PART	X2t (MPa)	X2c (MPa)	S12 (MPa)	S23 (MPa)	S31 (MPa)	ENKINK (J/m^2)	ENA (J/m^2)	ENB (J/m^2)	ENT (J/m^2)	ENL (J/m^2)		
CFRP	70	200	80	80	80	75100	50100	478	900	900		

Resin pocket (MAT_024) parameters are reported in Table 3.

Contact force and plate deflection were collected from the reaction force between the impacting mass and the plate, and from displacement of the impacting mass, respectively. Using these output data, the force–displacement curves were obtained via MATLAB elaboration.

Results and discussion

Force-displacement curves for experimental tests are reported in Figure 16.

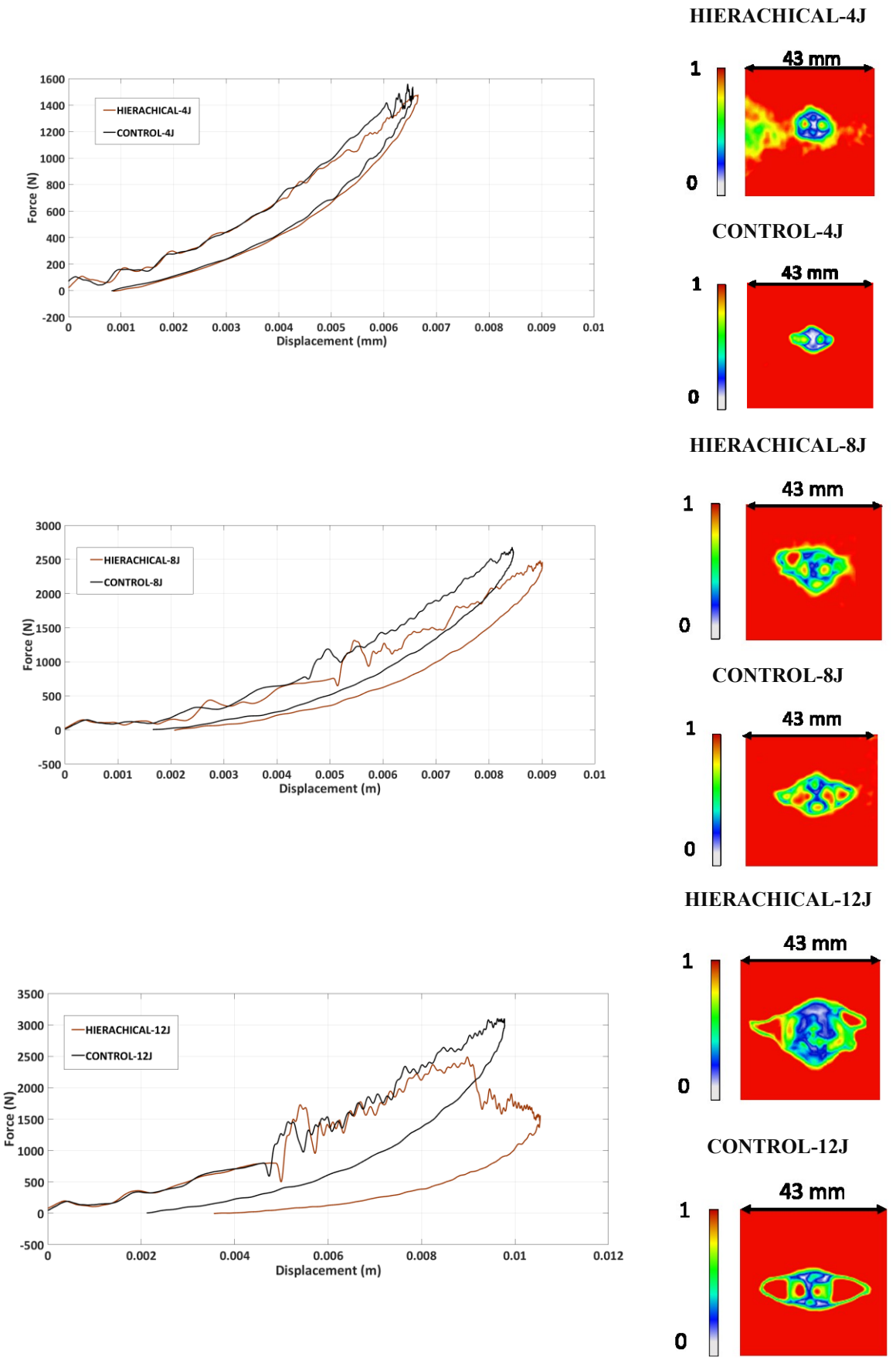

Figure 16-Force-Displacement curves and relative C-scan for experimental tests where the label HIERACHICAL corresponds to the 3D hierarchical CFRP samples and CONTROL to the traditional CFRP. The relative energy is reported for each curve.

To investigate the inner damage generated during the impact, an Ultrasonic Non-Destructive Technique (NDT) was used to evaluate the damaged area extension. C-scan images were obtained using a 5 MHz Phased Array Transducer with 128 Elements (National Instrument). The difference in terms of normalised amplitude in 16-bit colour scale is reported Figure 16 where the C-scan results are reported for each plate. In order to evaluate the damage topology, pseudo-plasticity effectiveness and crack distribution along the 3D hierarchical CFRP samples, a Computed Tomography (CT) scan was performed on all the impacted samples (bio-inspired and control). The output images are reported in Figure 17. All the images were collected using the same view, analysing a portion of the impacted area of the laminate.

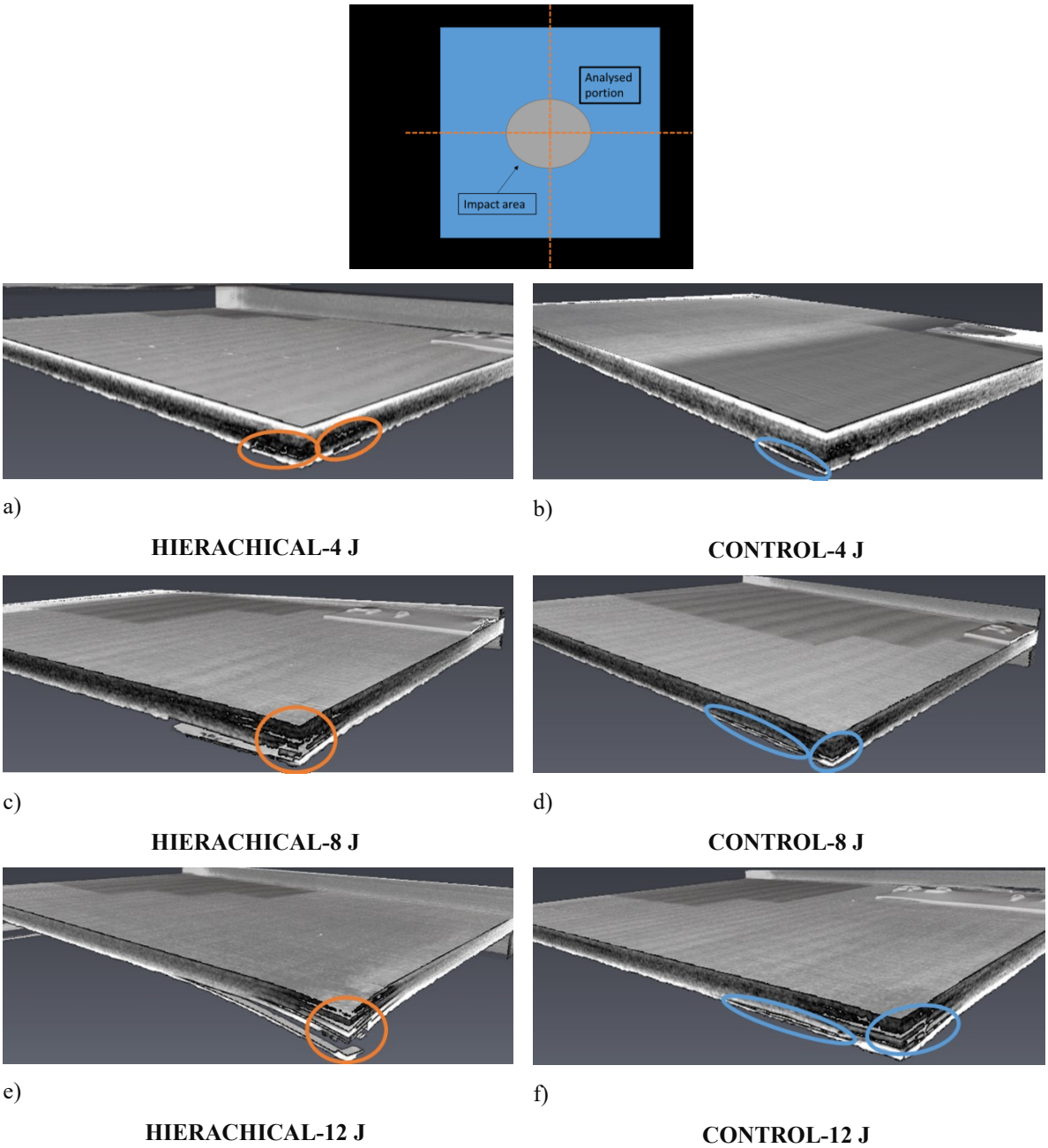

Figure 17- CT scan damage detection technique of the impacted samples: (a, c, e) 3D hierarchical samples impacted at 4J, 8J and 12 J respectively and (b, d, f) traditional CFRP samples impacted at 4J, 8J and 12J respectively Scanned area of the samples (50mm x 50mm) and the analysed portion are indicated in the reported scheme.

Statistical data for the impacted samples are reported in Table 8.

Table 8-Statistical data from impact campaign. 4J, 8J and 12J are the impact energies and the impact parameters of Peak Force, Maximum Displacement, Absorbed Energy and Delaminated area are reported

REFERENCE				
Energy (J)	**Peak Force (N)**	**Max Displacement (mm)**	**Absorbed Energy (J)**	**Delaminated Area (mm^2)**
4	***1670***	***0.00661***	***1.3176***	***95.63***
8	***2805***	***0.00824***	***2.8857***	***225.76***
12	***3271***	***0.00962***	***5.6752***	***275.63***
HIERACHICAL				
Energy (J)	**Peak Force (N)**	**Max Displacement (mm)**	**Absorbed Energy (J)**	**Delaminated Area (mm^2)**
4	***1479***	***0.00661***	***1.3339***	***125.73***
8	***2610***	***0.00883***	***3.1581***	***238.59***
12	***2613***	***0.0105***	***9.4788***	***450.82***

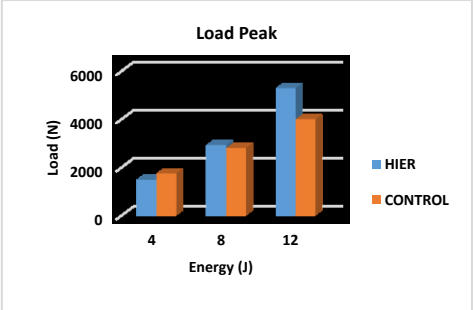

a)

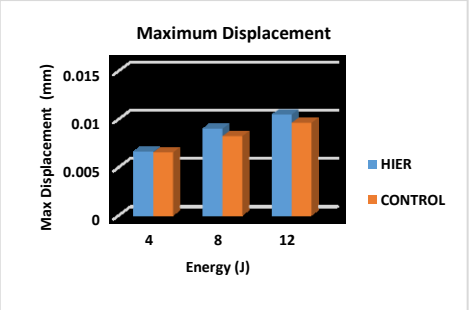

b)

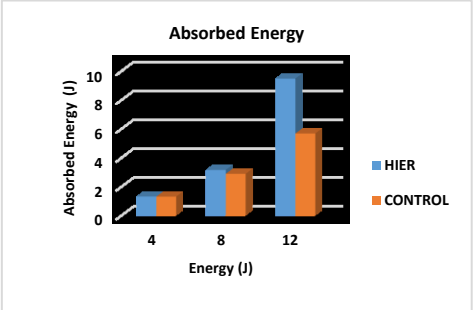

c)

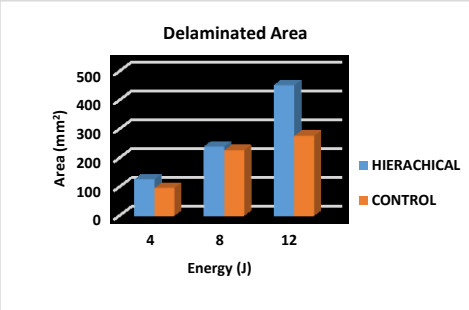

d)

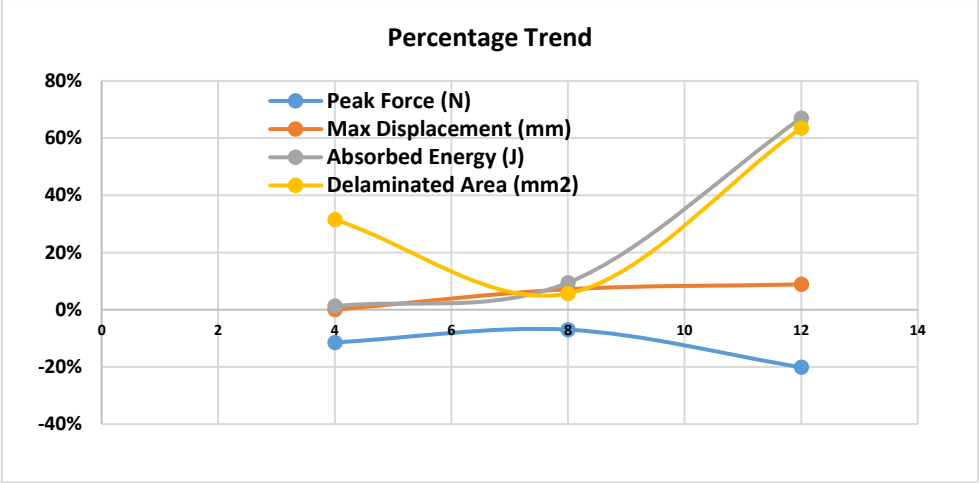

f)

Figure 18- Statistical data charts on impacted data for 4J, 8J and 12J impacts for control and 3D hierarchical CFRP sets: a) maximum contact force, b) maximum displacement, c) absorbed energy, d) damaged area extension and f) percentage variation of each statistical parameter.

From Figure 18, it is clear that at different impact energies, the impact behaviour and the relative pseudo-plastic effect exhibited by the bio-inspired samples is significantly different to the control samples. Considering the impacts at 4J, no difference in terms of impact response is reported for maximum displacement (+0.006%) and absorbed energy (+1%) reported in Figure 18.b and Figure 18.c. This is because pseudo-plastic features activation is restricted by the small impact energy amount introduced into the sample. However, it is still possible to notice differences in terms of peak force and delaminated area (Figure 18.a and Figure 18.d), with a percentage variation of -11% and +31% respectively due to the presence of the pattern of discontinuities that decreases mechanical properties, generating wider damaged area as shown in C-scan images (see Figure 16). CT-scanning (Figure 17.a and Figure 17.b) confirms this trend showing a wider damaged area for the hierarchical samples with signs of zig-zag crack propagation throughout the discontinuities pattern in a non-uniform damage propagation (orange circles). On the contrary, traditional CFRP show a classical reversed cone damage failure mode [52] with a symmetrical distribution of the damaged area, mainly constituted by delamination (blue circles). For results for the impact at 8J, the activation of pseudo-plastic abilities such as crack deflection and fibres pull-out, and the consequent enhanced toughness and strain at failure lead to a higher amount of energy absorbed during the LVI event. Even though the load peak is reduced by -7%, the effects of these mechanism are clear on the maximum displacement, absorbed energy and delaminated area that show a variation in comparison with unprocessed CFRP of +7%, +9% and +6% respectively. As for the internal defects, the C-scan images show a wide damaged area inside the sample with a circular shape around the impact area while, for the control samples, the damage is displayed as a delamination areas in cross-ply configuration [53]. By comparing CT-scan images between the two configurations, it is possible to identify the crack deflection mechanism following the resin pattern which lead to a fragmentation of the inner portion of the laminate. This different behaviour explains the

increased absorbed energy and larger damage extension in the bioinspired samples compared to the controls ones. In control samples, delamination is clearly identified in the laminate's body and for this reason, no signs of damage are visible on the impacted surface of the sample. It is important to underline that the 3D hierarchical CFRP structures impacted at 8J show evident signs of damage in correspondence to the indentation point. This is an important warning sign that the structure is able to provide that allows an immediate identification of the damaged portion without the use of NDT.

These results and evaluations are also verified in the 3D hierarchical samples impacted at 12J, where the higher impact energy amplifies the effects of pseudo-plasticity. Reporting a load peak reduction of -20% and an increase in maximum displacement of +9%, this typology is able to absorb high amounts of impact energy (+67%). This value is consistent with the energy absorption data found for static tests and is confirmed by the C-scan images that report increased damaged areas inside the laminate (+64%) but limiting the damaged area in a circular portion surrounding the indentation. Analysing CT scan images, it is clear that pseudo-plastic effects were activated and exploited to generate numerous cracks that follow the resin patterns. Several fragmented areas are observed in the inner structure with a consistent presence of indentation and structure failure, visible from the external surfaces of the samples. In contrast, control samples, show a traditional BVID that is not visible without the use of NDT analyses. The introduction of 3D hierarchical patterns into CFRP structures demonstrates its effectiveness in increasing toughness and strain at failure, generating a wider and fragmented damaged area in comparison with traditional laminates when undergoing LVI event. Moreover, the activation of crack deflection along the samples thickness, in addition to the pull-out of carbon fibres from the crack surfaces increases the absorbed energy of the bio-inspired structure. Numerical modelling confirms these energy absorption improvement, reporting a good correlation with experimental results as observed in Figure 19 and Figure 20.

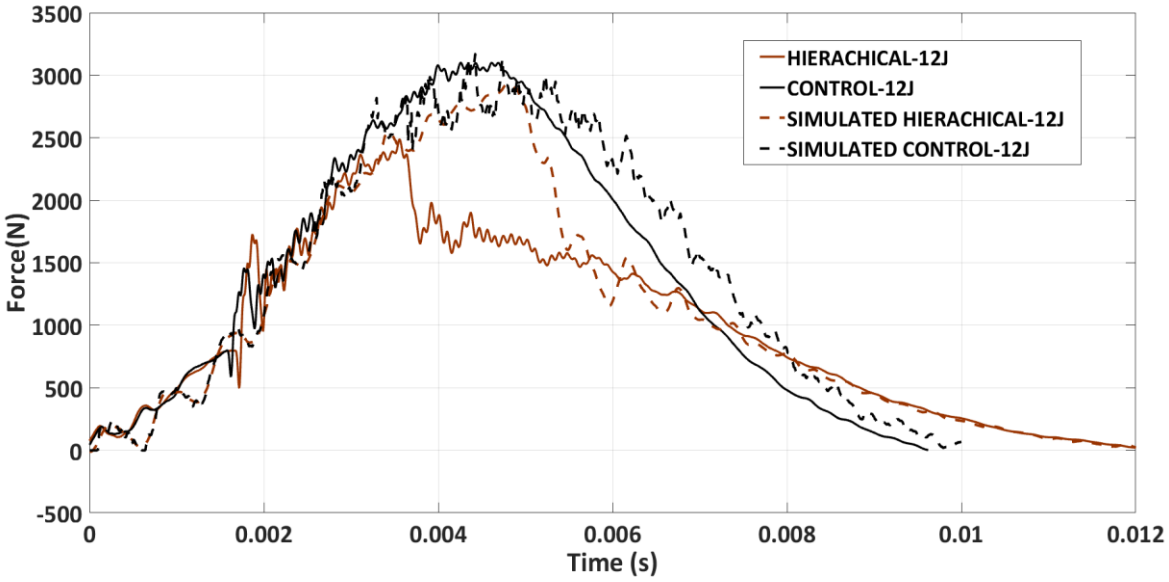

Figure 19-Force-time plot for 12J impacts results reporting numerical FEM results for the same impact event

Numerical model is reported only for 12 J case since it is the case at higher energy and the most critical conditions in terms of pseudo-plastic behaviour and failure mechanism involved. A similar impact behaviour is observed in terms of stiffness and strength between numerical and experimental results for hierarchical CFRP even if an overestimation of maximum force (+20%) is reported due to the complex fracture mechanism involved during pseudo-plastic behaviour simulation. The comparison between numerical and experimental data of traditional laminated composite shows an excellent match of stiffness and maximum contact force (+2%). In order to analyse the performance of the hierarchical material in impact energy absorption and the maximum displacement reached during the impact event, force-displacement comparison plot between experimental and numerical impact tests is reported in Figure 21.

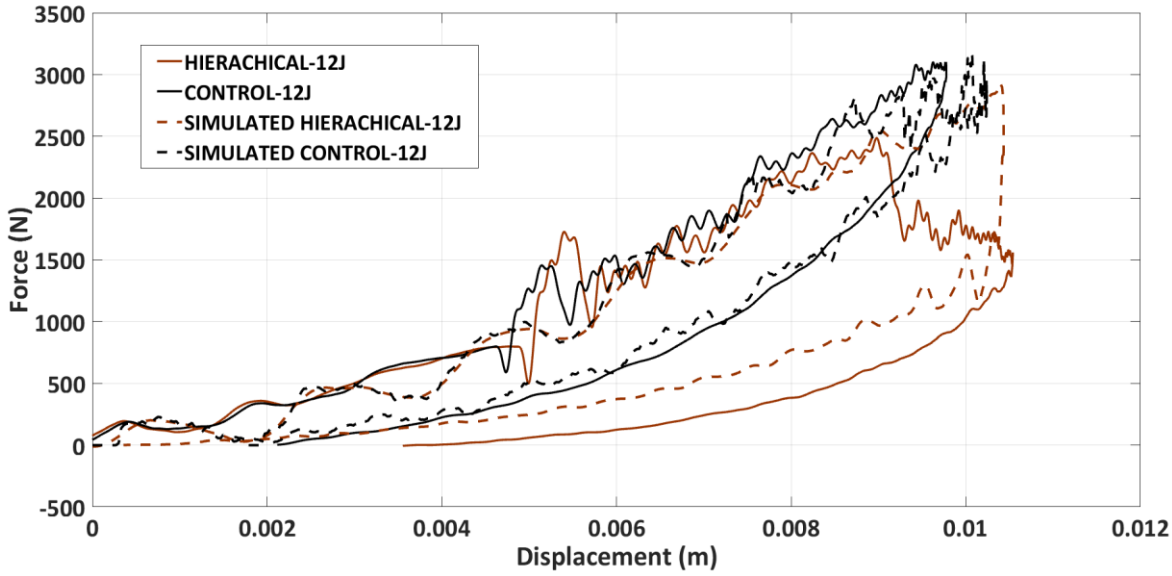

Figure 20- Force-displacement plot for 12J impacts results reporting numerical FEM results for the same impact event

As it is possible to observe from the graph, the pseudo-plasticity is completely taken into account from the numerical model reporting matching maximum displacement between numerical and experimental response of hierarchical composite structure with a difference of -1%. Similarly, impact responses of traditional laminates are similar in terms of maximum displacement with a variation of +6% for numerical data over experimental. Analysing the absorbed energy, the traditional laminate shows similar values between the numerical and experimental (-8% of variation),while absorbed energy prediction for the hierarchical material shows differences in terms of damage evolution that affects the curves fitting due to the complex nature of failure mechanisms involved (crack propagation, pull-out and fragmentation). Nevertheless, the numerical model is able to predict the global impact energy absorption of the hierarchical material with a difference of -4% in comparison with experimental.

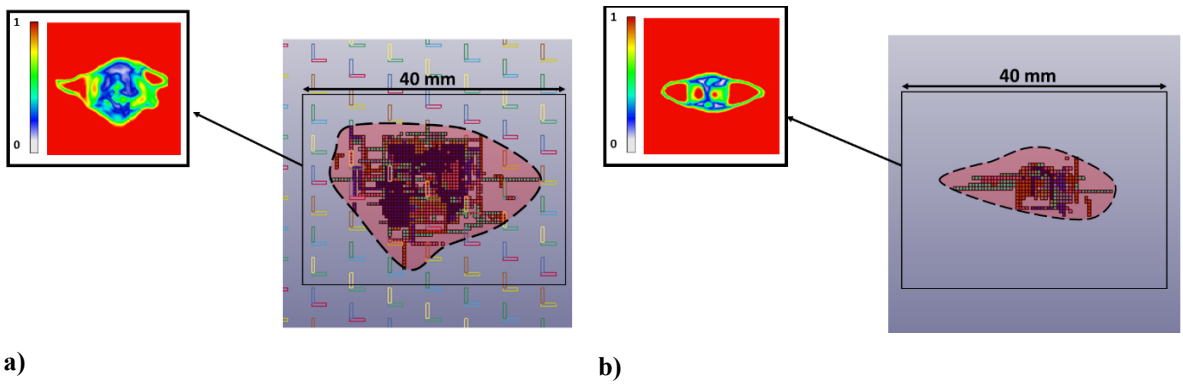

Figure 21- Damage comparison between eroded elements of numerical model and C-scan damage images of impacted samples: a) hierarchical and b) control

In order to confirm the numerical model reliability in damage mode prediction, eroded elements evaluation is used to compare damage within the numerical hierarchical and traditional laminates with damaged areas detected within the real structures using C-scan. Their comparison is reported in Figure 21 where it is possible to observe damaged areas with similar shape and extension for both experimental and numerical cases, demonstrating the reliability of the numerical model in predicting impact response, damaged area extent and severity, and impact energy absorption ability of the 3D bio-inspired hierarchical CFRP.

5 Conclusions

This paper presents new and optimised of Discontinuous Carbon Fibre Reinforced Polymers (DCFRPs) by mimicking biological hierarchical structures in order to improve impact response while preserving high-formability of composite laminates. Indeed, while it is well known that simple discontinuous fibres lead to a detriment of in-plane mechanical properties, by arranging these discontinuities in specific three-dimensional patterns it is possible to improve the toughness and strain at failure by enabling additional pseudo-plastic dissipative mechanisms such as crack deflection and fibres pull-out, thus preventing the typical brittle failure of composite laminates.

Experimental and numerical results are reported under static (three-point bending tests) and dynamic (Low Velocity Impacts) loading conditions. The effectiveness of several manufacturing alternatives for the introduction of discontinuities patterns and their main design parameters were evaluated. A Direct Approach manufacturing procedure with a 50 mm long elemental cell was chosen over an Indirect Approach (IA) for the discontinuities pattern design since IA showed significant loss in mechanical properties (at least 20%) when compared to traditional CFRP. Three-points bending tests were carried out on the bio-inspired and traditional unidirectional CFRP samples to evaluate the difference in terms of mechanical response. Small variations of around +4%,-4%, -1.2% and +1.2% for strain at failure, maximum strength, flexural modulus and toughness respectively were found between the two configuration. The bioinspired structures displayed an effective pseudo-plastic behaviour with no signs

of brittle failure in the laminate. Based on these results, the hierarchical concept was extended to a more complex CFRP laminate configuration (cross-ply stacking sequence) and the mechanical response investigated using a three-point bending methodology. Significant increases in toughness and strain at failure of +24% and +44% alongside a reduction in terms of maximum strength and flexural modulus of -20% and -8.4% was reported, confirming the effectiveness of the discontinuities pattern in increasing the CFRP toughness. A good correlation between experimental and simulated results was found, with excellent accuracy in strength and modulus prevision. In addition, in order to demonstrate the efficiency of pseudo-plasticity in dynamic loading conditions, a LVI impact campaign at several impact energies was carried out. Impact results showed an increase of +67% and +9% for absorbed energy and maximum displacement respectively. Good agreement was shown with numerical impact results with a variation in terms of -4% in the prevision of the absorbed energy of the 3D hierarchical structure allowing the use of this material in crashworthiness application when high energy dissipation is required.

In conclusion, this discontinuous bio-inspired material can be used in advanced applications and complex manufacturing process where impact toughness and high-performance are the main objective during the operative life of the structure.

6 References

[1] Feraboli P, Masini A, Taraborrelli L, Pivetti A. Integrated development of CFRP structures for a topless high performance vehicle. Composite Structures. 2007;78:495-506.

[2] Neoh E-T. Drape properties of thermostetting prepregs: Massachusetts Institute of Technology, 1992.

[3] Pinto F, White A, Meo M. Characterisation of ductile prepregs. Applied Composite Materials. 2013;20:195-211.

[4] Tsuji N, Springer GS, Hegedus I. The drapability of aligned discontinuous fiber composites. Journal of composite materials. 1997;31:428-65.

[5] Chang IY, Pratte JF. LDF™ thermoplastic composites technology. Journal of Thermoplastic Composite Materials. 1991;4:227-52.

[6] Gutowski T, Hoult D, Dillon G, Gonzalez-Zugasti J. Differential geometry and the forming of aligned fibre composites. Composites Manufacturing. 1991;2:147-52.

[7] Simmons A. An analysis of the properties of carbon fibre aligned discontinuous prepreg tape. SAMPE, Baltimore (USA). 2012.

[8] Anderson TL. Fracture mechanics: fundamentals and applications: CRC press, 2017.

[9] Ilcewicz L, Murphy B. Safety & certification initiatives for composite airframe structure. 46th AIAA/ASME/ASCE/AHS/ASC Structures, Structural Dynamics and Materials Conference2005. p. 1877.

[10] Li VC, Wu H-C. Conditions for pseudo strain-hardening in fiber reinforced brittle matrix composites. Applied Mechanics Reviews. 1992;45:390-8.

[11] Rho J-Y, Kuhn-Spearing L, Zioupos P. Mechanical properties and the hierarchical structure of bone. Medical engineering & physics. 1998;20:92-102.

[12] Meyers MA, Chen P-Y, Lin AY-M, Seki Y. Biological materials: structure and mechanical properties. Progress in Materials Science. 2008;53:1-206.

[13] Li X, Wang J, Du J, Cao M, Liu K, Li Q, et al. Spear and shield: survival war between Mantis Shrimps and Abalones. Advanced Materials Interfaces. 2015;2.

[14] Chen P-Y, McKittrick J, Meyers MA. Biological materials: functional adaptations and bioinspired designs. Progress in Materials Science. 2012;57:1492-704.

[15] Barthelat F. Nacre from mollusk shells: a model for high-performance structural materials. Bioinspiration & biomimetics. 2010;5:035001.
[16] Barthelat F, Tang H, Zavattieri P, Li C-M, Espinosa H. On the mechanics of mother-of-pearl: a key feature in the material hierarchical structure. Journal of the Mechanics and Physics of Solids. 2007;55:306-37.
[17] Sun J, Bhushan B. Hierarchical structure and mechanical properties of nacre: a review. Rsc Advances. 2012;2:7617-32.
[18] Yourdkhani M, Pasini D, Barthelat F. Multiscale mechanics and optimization of gastropod shells. Journal of Bionic Engineering. 2011;8:357-68.
[19] Katti KS, Katti DR, Mohanty B. Biomimetic lessons learnt from nacre. Biomimetics Learning from Nature: InTech; 2010.
[20] Meyers MA, Lin AY-M, Chen P-Y, Muyco J. Mechanical strength of abalone nacre: role of the soft organic layer. Journal of the mechanical behavior of biomedical materials. 2008;1:76-85.
[21] Wang R, Suo Z, Evans A, Yao N, Aksay I. Deformation mechanisms in nacre. Journal of Materials Research. 2001;16:2485-93.
[22] Evans A, Suo Z, Wang R, Aksay I, He M, Hutchinson J. Model for the robust mechanical behavior of nacre. Journal of Materials Research. 2001;16:2475-84.
[23] Jackson A, Vincent JF, Turner R. The mechanical design of nacre. Proc R Soc Lond B. 1988;234:415-40.
[24] Lin AY-M, Meyers MA. Interfacial shear strength in abalone nacre. Journal of the mechanical behavior of biomedical materials. 2009;2:607-12.
[25] Barthelat F, Rabiei R. Toughness amplification in natural composites. Journal of the Mechanics and Physics of Solids. 2011;59:829-40.
[26] Faber KT, Evans AG. Crack deflection processes—I. Theory. Acta metallurgica. 1983;31:565-76.
[27] Czél G, Pimenta S, Wisnom MR, Robinson P. Demonstration of pseudo-ductility in unidirectional discontinuous carbon fibre/epoxy prepreg composites. Composites Science and Technology. 2015;106:110-9.
[28] Czél G, Jalalvand M, Wisnom MR. Demonstration of pseudo-ductility in unidirectional hybrid composites made of discontinuous carbon/epoxy and continuous glass/epoxy plies. Composites Part A: Applied Science and Manufacturing. 2015;72:75-84.
[29] Malkin R, Yasaee M, Trask RS, Bond IP. Bio-inspired laminate design exhibiting pseudo-ductile (graceful) failure during flexural loading. Composites Part A: Applied Science and Manufacturing. 2013;54:107-16.
[30] Gu GX, Takaffoli M, Hsieh AJ, Buehler MJ. Biomimetic additive manufactured polymer composites for improved impact resistance. Extreme Mechanics Letters. 2016;9:317-23.
[31] Narducci F, Pinho S. Exploiting nacre-inspired crack deflection mechanisms in CFRP via micro-structural design. Composites Science and Technology. 2017;153:178-89.
[32] Römer L, Scheibel T. The elaborate structure of spider silk. Prion. 2008.
[33] Jones RM. Mechanics of composite materials: CRC press, 2014.
[34] Petersen R. Discontinuous fiber-reinforced composites above critical length. Journal of dental research. 2005;84:365-70.
[35] Laspalas M, Crespo C, Jiménez M, García B, Pelegay J. Application of micromechanical models for elasticity and failure to short fibre reinforced composites. Numerical implementation and experimental validation. Computers & Structures. 2008;86:977-87.
[36] Zak G, Haberer M, Park C, Benhabib B. Mechanical properties of short-fibre layered composites: prediction and experiment. Rapid Prototyping Journal. 2000;6:107-18.
[37] Piggott MR. Short fibre polymer composites: a fracture-based theory of fibre reinforcement. Journal of composite materials. 1994;28:588-606.
[38] Otani LB, Pereira AHA, Melo JDD, Amico SC. Elastic Moduli characterization of composites using the Impulse Excitation. 2014.
[39] Begley MR, Philips NR, Compton BG, Wilbrink DV, Ritchie RO, Utz M. Micromechanical models to guide the development of synthetic ‘brick and mortar’composites. Journal of the Mechanics and Physics of Solids. 2012;60:1545-60.

[40] Barthelat F. Designing nacre-like materials for simultaneous stiffness, strength and toughness: Optimum materials, composition, microstructure and size. Journal of the Mechanics and Physics of Solids. 2014;73:22-37.
[41] Wilson CD. Linear elastic fracture mechanics primer. 1992.
[42] He K, Hoa S, Ganesan R. The study of tapered laminated composite structures: a review. Composites Science and Technology. 2000;60:2643-57.
[43] Friedrich K. Application of fracture mechanics to composite materials: Elsevier, 2012.
[44] Nakanishi Y, Hana K, Hamada H. Fractography of fracture in CFRP under compressive load. Composites Science and Technology. 1997;57:1139-47.
[45] Tao J, Sun C. Influence of ply orientation on delamination in composite laminates. Journal of composite materials. 1998;32:1933-47.
[46] Ginzburg D, Pinto F, Iervolino O, Meo M. Damage tolerance of bio-inspired helicoidal composites under low velocity impact. Composite Structures. 2017;161:187-203.
[47] Hallquist JO. LS-DYNA theory manual. Livermore software Technology corporation. 2006;3:25-31.
[48] Hallquist JO. LS-DYNA keyword user's manual. Livermore software Technology corporation. 2007;970:299-800.
[49] Manual L-DKUs. vol. II. Livermore Software Technology Corporation (LSTC). 2013.
[50] Pinho ST, Robinson P, Iannucci L. Fracture toughness of the tensile and compressive fibre failure modes in laminated composites. Composites Science and Technology. 2006;66:2069-79.
[51] Pinho S, Iannucci L, Robinson P. Physically based failure models and criteria for laminated fibre-reinforced composites with emphasis on fibre kinking. Part II: FE implementation. Composites Part A: Applied Science and Manufacturing. 2006;37:766-77.
[52] Abrate S. Impact on laminated composite materials. Appl Mech Rev. 1991;44:155-90.
[53] Wisnom M. The role of delamination in failure of fibre-reinforced composites. Phil Trans R Soc A. 2012;370:1850-70.